SKS splitting and seismic anisotropy beneath the Mid-Atlantic Appalachians using data from the MAGIC FlexArray experiment

John C. Aragon

Advisor: Maureen D. Long

Second Reader: Jeffrey Park

5 May 2017

A Senior Thesis presented to the faculty of the Department of Geology and Geophysics, Yale University, in partial fulfillment of the Bachelor's Degree.

Abstract

North America's eastern passive continental margin has been modified by several cycles of supercontinent assembly. Its complex surface geology and distinct topography provide evidence of these events, while raising fundamental questions about the extent and style of deformation in the continental crust and upper mantle during past episodes of rifting and mountain building. We evaluate record sections of *SKS* arrivals and measure splitting of *SKS* phases using seismic data collected by the Mid-Atlantic Geophysical Integrative Collaboration (MAGIC), an EarthScope and GeoPRISMS-funded cohort of seismologists, geodynamicists, and geomorphologists. MAGIC seismologists from Yale and The College of New Jersey constructed 28 temporary seismic observatories in a linear path from western Ohio to coastal Virginia, which collected broadband seismic data from October 2013 to October 2016. *SKS* splitting parameters along the array reveal distinct regions of upper mantle anisotropy. Stations to the west and within the Appalachian range exhibit delay times of about 1.0 s and fast directions parallel to the strike of the mountains (60° from N). Stations immediately to the East of the mountains exhibit more complicated splitting, indicating a sharp change in upper mantle anisotropy. Easternmost stations exhibit weaker splitting, higher occurrences of null *SKS* arrivals, and a clockwise rotation of the average fast direction, suggesting the possibility of multilayered anisotropy. Record sections of *SKS* arrivals at MAGIC stations and stereo plots of single-station splitting patterns work to highlight these transitions. When combined with previous work, patterns in *SKS* splitting suggest that lithospheric deformation associated with Appalachian orogenesis contributes the observed anisotropy across the Mid-Atlantic Appalachians.

1. Introduction

The Mid-Atlantic Appalachians are a result of a Paleozoic accretionary orogen on the eastern margin of Laurentia near the end of a complex Wilson cycle (eg., Cawood and Buchan, 2007; Hatcher, 2010; Hoffman et al., 2016). This cycle began with the breakup of supercontinent Rodinia ~825–550 Ma. Later, between 600 Ma and 400 Ma, the Iapetus Ocean opened between Laurentia, Baltica, and Avalonia. The Wilson cycle completed with the Taconian, Acadian, and Alleghanian orogenies ~470-300 Ma. Subsequently, Laurentia collided with the continent of Gondwana to form the supercontinent Pangaea. Later rift faulting and sedimentation eroded the surface of the Appalachians around 230 Ma. These rifts were intruded by mantle derived lavas ~200 Ma, and seafloor spreading in the proto-Atlantic basin began ~170 Ma, creating the passive continental margin we see today.

Our current understanding of the tectonic evolution of eastern North America does much to explain the region's complicated geology and physiography, yet many basic questions about the structure of the underlying mantle remain. Unresolved topics include the extent and nature of continental lithospheric deformation associated with past episodes of orogenesis and rifting, the geometry of present-day deformation in the asthenospheric upper mantle, and the persistent nature of Appalachian topography. These questions are being investigated by the Mid-Atlantic Geophysical Integrative Collaboration (MAGIC), an EarthScope and GeoPRISMS-funded project that involves a joint effort between seismologists, geodynamicists, and geomorphologists. Here we present observations of seismic anisotropy using data from the MAGIC broadband FlexArray seismic experiment (Long and Wiita, 2013).

SKS splitting found in seismic data is an unambiguous indicator of anisotropy and a powerful tool for identifying deformation in the Earth's mantle (eg., Long, 2010). Because it is a core phase, the initial polarization of an SKS phase entering the mantle beneath a station is controlled by the P-to-S conversion at the core-mantle boundary. This makes the SKS phase an ideal choice for measuring seismic anisotropy because observed splitting of the *SKS* phase is constrained to the receiver side and the initial polarization of the phase matches the backazimuth between the event and station (eg., Long and Silver, 2009). When a shear wave propagates through an anisotropic medium, it is split into two orthogonally
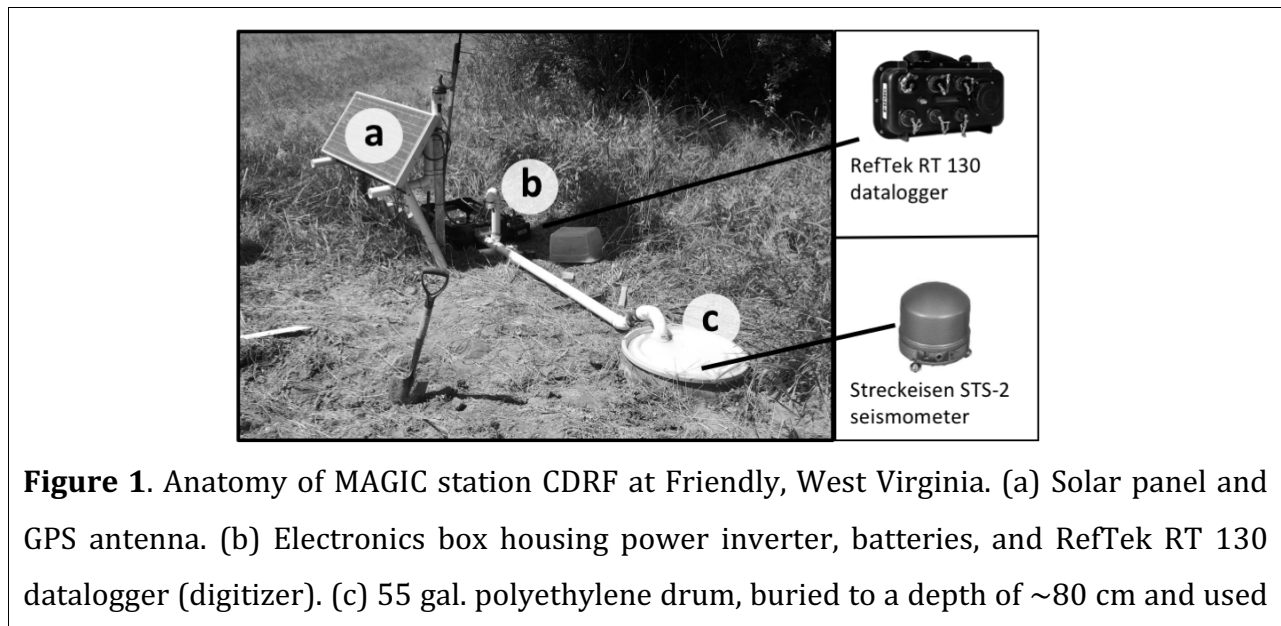
polarized components, and when ground motion from SKS arrivals is recorded by broadband instruments, mantle anisotropy can be measured. Splitting parameters contain a fast direction (ϕ) and delay time (δt). The fast direction corresponds to the orientation of the fast quasi-S phase component, and the delay time corresponds to the accumulated delay between the fast and slow components. In the upper mantle, anisotropy generally results from the lattice preferred orientation of individual mineral grains in deformed rocks (eg., Karato et al., 2008).

Recent work using data from the Transportable Array (TA) component of EarthScope's USArray (USArray, 2003) has greatly increased the spatial resolution of observed anisotropy in the eastern U.S. and southeastern Canada (Long et al., 2016). The TA deployment represents the most comprehensive set of seismic data from North America to date. Long et al. (2016) identify regional patterns based on *SKS* splitting behavior. General observations include a NE-SW trend to fast directions for much of the Southeast, especially west of the Appalachian Mountains, an E-W trend to measured fast directions in the Northeast and southeastern Canada, and a high number of null *SKS* arrivals east of the Appalachians in the southern Atlantic Coastal Plain. The authors also found a strong tendency for stations seated within the high topography of the Appalachian mountain chain, stretching through northeastern Alabama to Pennsylvania, to yield fast directions parallel to the strike of the mountains.

Here we present 397 high quality *SKS* splitting parameters from ~105 events, and record sections from five seismic events with very clear *SKS* arrivals. These data were recorded at 28 MAGIC seismic observatories, optimally placed to observe changes in *SKS* splitting patterns between the regions of coherent splitting identified by Long et al. (2016). While TA stations were at a nominal spacing of ~75 km from one another, MAGIC stations maintained a spacing of ~25 km, with stations in areas of particular interest (eg., the Valley and Ridge province of West Virginia) spaced as close as 10 km to 15 km apart. This spacing is significant, given the excellent lateral resolution produced from *SKS* splitting analysis techniques (Long and Silver, 2009). Comparison of splitting parameters from the MAGIC array, combined with record sections from events with clear *SKS* arrivals give an unprecedented resolution to transitions in upper mantle anisotropy in our region of study.

2. Data and methods

Data collection began in October of 2013 with the construction of 13 seismic observatories in Virginia and West Virginia, using Trillium 120 broadband sensors and Taurus digitizers made by Nanometrics and owned by Yale University. The sighting and building of stations was led by MAGIC seismologists Maureen D. Long from Yale University and Margaret H. Benoit from The College of New Jersey, and carried out by student volunteers from Yale, The College of New Jersey, Virginia Polytechnic Institute, and Princeton. Stations (Figure 1) were engineered to follow the design of previous work with the 2005-2010 High Lava Plains FlexArray experiment (Fouch, 2006). In October of 2014, the MAGIC experiment received 28 Streckeisen STS-2 broadband sensors and RefTek RT 130 digitizers from the USArray FlexArray pool of portable seismic instruments to replace university owned instruments at existing stations and extend the array with equipment for an additional fifteen stations. Figure 2a displays the completed array of 28 stations, which stretched from Ohio's Central Lowland province to the Atlantic Coastal Plain. The linear array was nearly perpendicular to the strike of the Appalachian Mountains, allowing MAGIC stations to sample ground motion across a range of topographies (Figure 2b) such as the Appalachian Plateau, Ridge and Valley, Great Valley, Blue Ridge, and Piedmont physiographic regions (Fenneman and Johnson, 1946).

Figure 1. Anatomy of MAGIC station CDRF at Friendly, West Virginia. (a) Solar panel and GPS antenna. (b) Electronics box housing power inverter, batteries, and RefTek RT 130 datalogger (digitizer). (c) 55 gal. polyethylene drum, buried to a depth of ~80 cm and used

to house a Streckeisen STS-2 seismometer.

Fieldwork, in the form of data collection and station maintenance, continued until October 2016, when the array was demobilized. As data were collected, we inspected waveforms for signs of instrumentation failure and processed files for submittal to the Incorporated Research Institutions for Seismology (IRIS) Data Management Center. After data were archived, we used the National Earthquake Information Center (NEIC) catalog to select ~500 earthquakes of magnitude 5.8 Mw or greater, that were at epicentral distances between 90° and 130° from individual stations. Of these, ~107 earthquakes from a range of backazimuths offered well resolved *SKS* parameters (Figure 3a). A histogram of the data set's backazimuthal coverage (Figure 3b) reveals the limiting factor of sparse coverage between 50° and 250° due to the distribution of global seismicity.
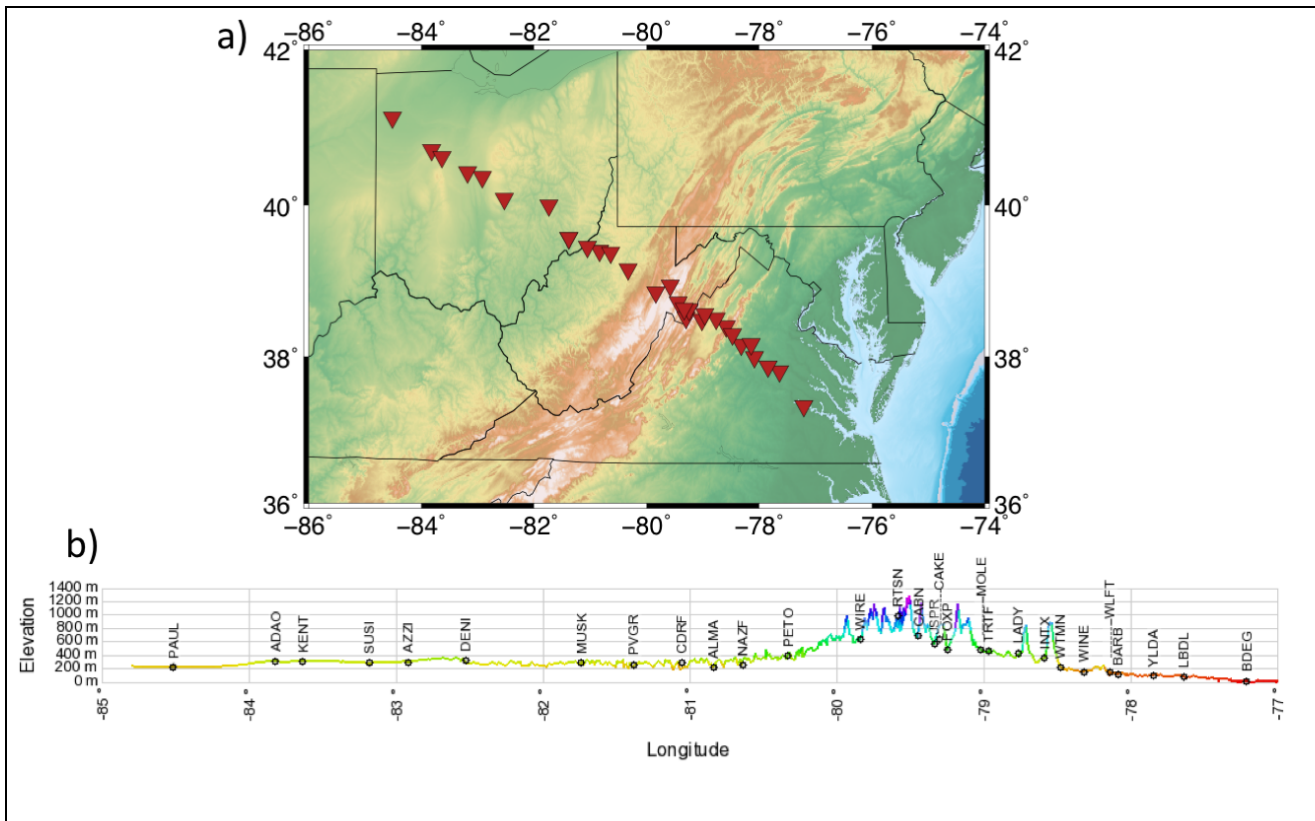
Figure 2. (a) Map of MAGIC station locations (red triangles) in Ohio, West Virginia, and Virginia made with GMT (Wessel et al., 2015). (b) Elevation profile of magic array plotted against longitude. Y-axis exaggerated by a factor of ~46. Stations (⊕) are labeled with four-character station codes.
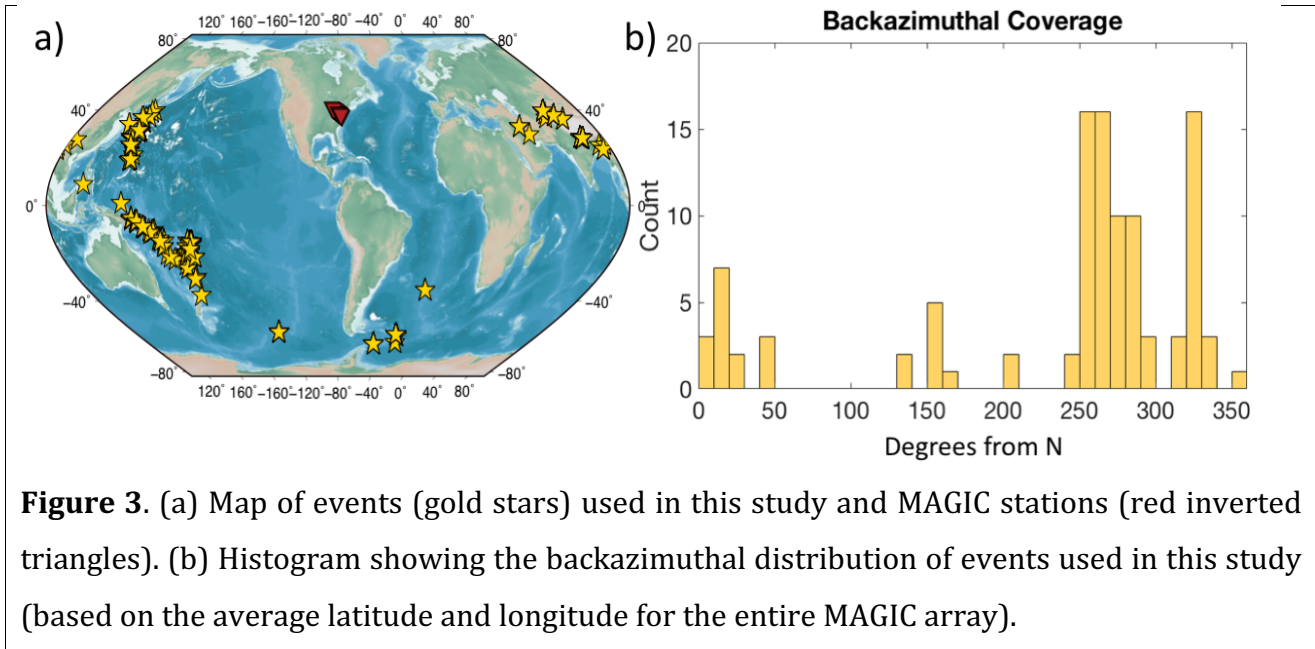
Figure 3. (a) Map of events (gold stars) used in this study and MAGIC stations (red inverted triangles). (b) Histogram showing the backazimuthal distribution of events used in this study (based on the average latitude and longitude for the entire MAGIC array).
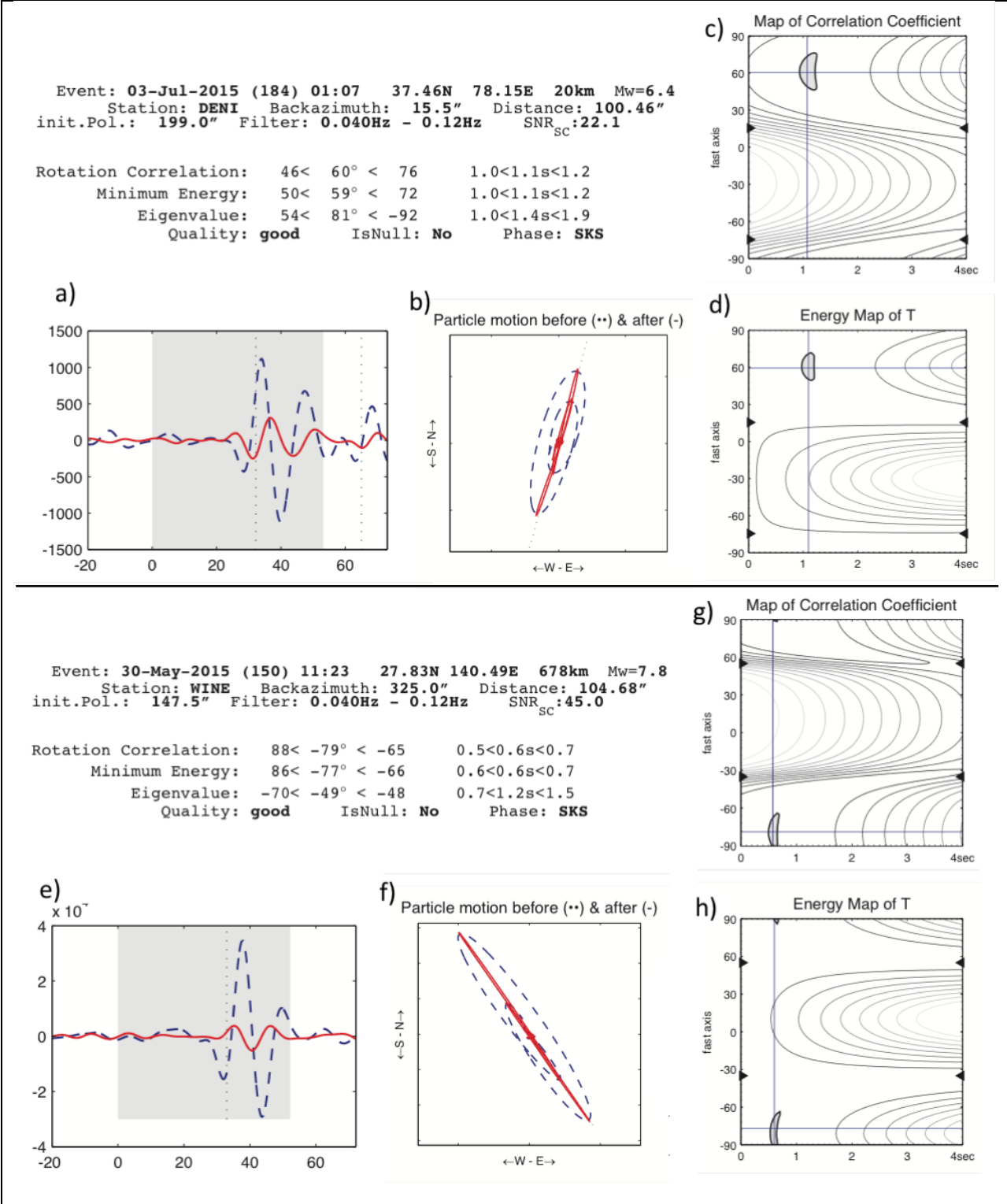
In preparation for *SKS* analysis, data were bandpass filtered to retain energy periods between 8 and 25 seconds. Splitting parameters, fast direction (ϕ) and delay time (δt), were then measured using the SplitLab software (Wüstefeld et al., 2008). The rotation-correlation and transverse component minimization methods were applied to all apparent SKS arrivals in accordance with previous work (Long et al., 2010; Long and Silver, 2009; Wagner et al., 2012), and the results can be directly compared. Measurements having 95% confidence regions of up to $\pm20°$ in ϕ and ±0.5 s in δt were marked "good" and those with $\pm30°$ in ϕ and ±0.5 s in δt were marked "fair." Only "good" and "fair" measurements are reported here. Figure 4 gives two examples of "good" quality nonnull (split) measurements using diagnostic plots from SplitLab.

SKS arrivals with a high signal-to-noise ratio on both the radial and transverse components and a linear uncorrected particle motion were designated as "null." Figure 5 displays two examples of "good" quality null measurements with quite linear uncorrected particle motion and very low noise on the transverse component. Null measurements with slightly less than linear uncorrected particle motion, yet still exhibiting low noise on the transverse component were designated as "fair." Only "good" and "fair" null measurements are reported here.

Data were also prepared for use in record section to show lateral variations in *SKS* arrivals along the MAGIC array path. Five events from a range of backazimuths were selected for having clear *SKS* arrivals. The waveforms were filtered to retain energy between 8 s and 25 s and rotated to the backazimuth between the event and station along the great circle path using the Seismic Analysis Code (SAC, 1995). Waveforms were then imported to MATLAB (MATLAB, 2012) using SACLAB by Michael Thorne (Thorne, 2015) and aligned to the expected *SKS* arrival based on the IASP91 standard Earth model and plotted according to the observed initial particle motion found in SplitLab. For the majority of waveforms, no valid splitting parameters were observed because *SKS* splitting is a low yield measurement that is difficult to constrain (eg., Long and Silver, 2009), making record sections of pronounced *SKS* arrivals a valuable complementary tool to *SKS* splitting for evaluating lateral changes in anisotropy.

Since data were collected in batches at six month intervals, *SKS* splitting parameters were measured throughout the experiment and preliminary findings were reported at American Geophysical Union Fall meeting in 2015 and 2016 (Aragon et al., 2015; Aragon et al., 2016).

Figure 4. Examples of two nonnull splitting measurements, taken from SplitLab (Wüstefeld et al., 2008). Top panels (a-d) illustrate splitting parameters for an event on July 3, 2015, originating from Xinjiang, China at MAGIC station DENI (Denison University at Granville,
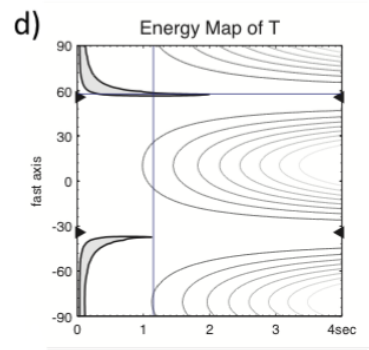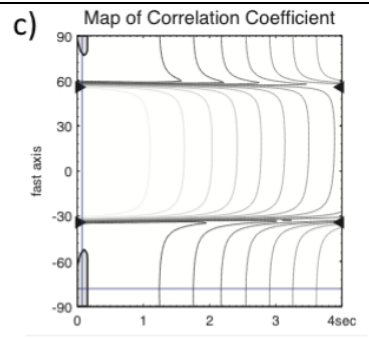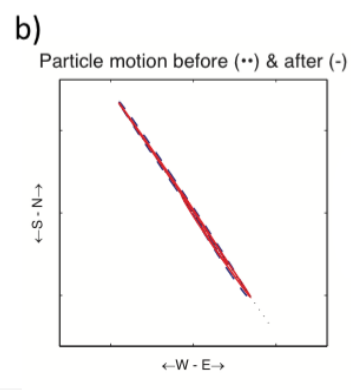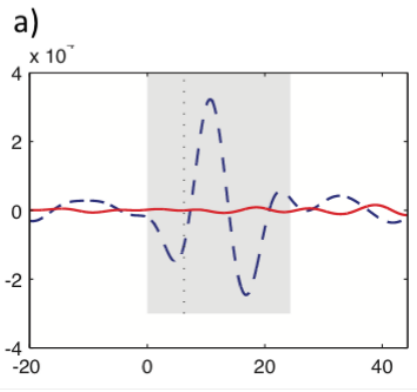
Ohio). (a) A window displaying the uncorrected radial (blue dashed line) and transverse (red solid line) component energies, the time window used in calculating splitting parameters (grey box), and the expected SKS arrival (vertical dashed line). It is clear the arrival exhibits transverse component energy above the level of noise. (b) Plot showing the uncorrected (blue dashed line) and corrected (red solid line) (meaning that the effects of splitting have removed using the transverse component minimization method) particle motions obtained using the transverse component minimization method. The uncorrected particle motion is elliptical and the corrected particle motion is nearly linear. The backazimuth is plotted with a grey dotted line. (c) Splitting parameter estimates for ϕ and δt using the rotation-correlation method are indicated with a cross on the contour plot of transverse component energy. The 95% confidence region for splitting estimates is indicated with a shaded region. (d) Splitting parameter estimates (plotted as in Figure 4c) using the transverse component minimization method (referred to as Minimum Energy within SplitLab). As with all high-quality measurements, the best fitting parameters from both methods agree. The rotation correlation method gives a fast direction of $\sim 60°$ ($\phi = 46°$ $< 60° < 76°$) and a delay time of ~ 1.1 s ($\delta t = 1.0$ s < 1.1 s < 1.2 s). The transverse component minimization method gives a fast direction of $\sim 59°$ ($\phi = 50° < 59° < 72°$) and delay time of ~ 1.1 s ($\delta t = 1.0$ s < 1.1 s < 1.2 s). Bottom panels (e-h) follow the plotting convention of (a-d). This split SKS arrival is from an event on May 30, 2015, originating from Bonin Islands, Japan and recorded at MAGIC station WINE (Liberty, Virginia). (e) The clear SKS arrival with transverse component energy above the level of noise (as in Figure 4a). (f) Plot of particle motion that is initially weakly elliptical, but changes to nearly linear when corrected using the transverse component minimization method. (g) Splitting parameter estimates using the rotation correlation method. (h) Splitting parameter estimates using the transverse component minimization method. Similar estimates are given for both methods, making this a "good" measurement. The rotation correlation method yields a fast direction of $\sim$-79° ($\phi = 88° < $-$79° < $-$65°$) and a delay time of ~ 0.6 s ($\delta t = 0.5$ s < 0.6 s < 0.7 s). The transverse component minimization method gives a fast direction of $\sim$-77° ($\phi = 86°$ $< $-$77° < $-$66°$) and delay time of ~ 0.6 s ($\delta t = 0.6$ s < 0.6 s < 0.7 s). This measurement is near the minimum threshold for which δt can be resolved ($\delta t = 0.5$ s).
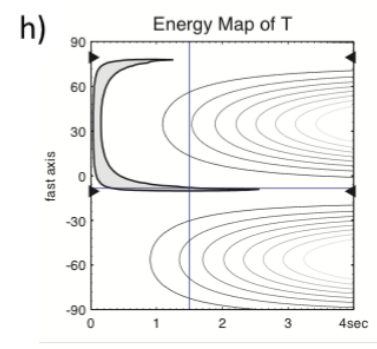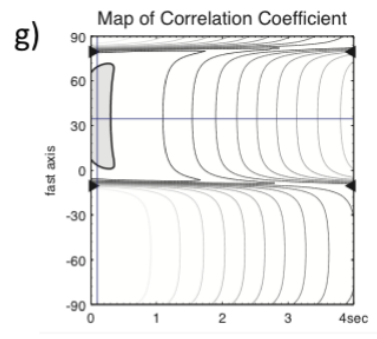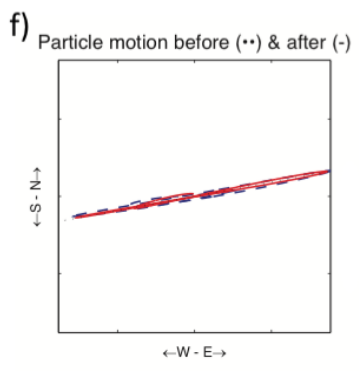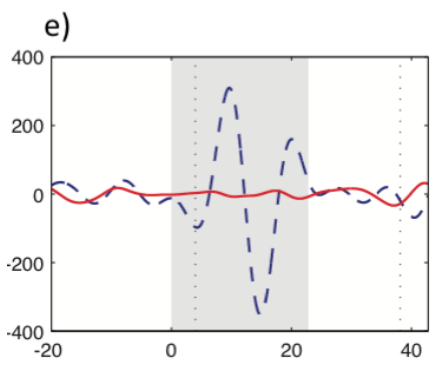
Event: **30-May-2015** (150) 11:23   27.83N 140.49E   678km   Mw=7.8
Station: **BDEG**   Backazimuth: **325.8"**   Distance: **105.86"**
init.Pol.:   **147.1"**   Filter: **0.040Hz – 0.12Hz**   SNR$_{SC}$:**50.3**

Rotation Correlation: 77< -78° < -54   0.0<0.1s<0.2
Minimum Energy: 58< 58° < -39   0.1<1.2s<2.0
Eigenvalue: 60< -34° < -37   0.1<1.9s<2.6
Quality: **fair**   IsNull: **Yes**   Phase: **SKS**

a)

b) Particle motion before (··) & after (-)

c) Map of Correlation Coefficient

d) Energy Map of T

Event: **10-Jul-2016** (192) 13:41   -15.03N -172.88E   8km   Mw=5.8
Station: **ALMA**   Backazimuth: **259.5"**   Distance: **101.02"**
init.Pol.:   **80.7"**   Filter: **0.040Hz – 0.12Hz**   SNR$_{SC}$:**46.4**

Rotation Correlation: 2< 35° < 72   0.0<0.1s<0.4
Minimum Energy: -13< -8° < 76   0.1<1.5s<2.6
Eigenvalue: -9< 78° < 80   0.1<0.9s<2.8
Quality: **good**   IsNull: **Yes**   Phase: **SKS**

e)

f) Particle motion before (··) & after (-)

g) Map of Correlation Coefficient

h) Energy Map of T

11

Figure 5. Two examples of null splitting measurements, taken from SplitLab (Wüstefeld et al., 2008). Plotting conventions are as in Figure 4. Top panels (a-d) illustrate null splitting parameters for an event on May 30, 2015, originating from Bonin Islands region of Japan, recorded at MAGIC station BDEG (Charles Lake, Virginia). (a) The SKS arrival is identified by high energy on the uncorrected radial component. Because this is a null arrival, the transverse component energy does not indicate energy above the level of noise. (b) Plot of particle motion. The uncorrected and corrected particle motion are nearly linear and aligned with the backazimuth (dotted line), which indicates null splitting. (c) Splitting parameter estimates using the rotation correlation method. (d) Splitting parameter estimates using the transverse minimization method. As with all high-quality null measurements, the error contours for each method do not yield a valid ϕ or δt. Bottom panels (e-h) illustrate null splitting parameters for an event on July 10, 2016, originating from the Samoa Islands Region, recorded at MAGIC station ALMA (Alma, West Virginia). (e) The SKS arrival is identified by high energy on the uncorrected radial component and low energy on the transverse component. (f) Plot of particle motion. The uncorrected and corrected particle motion are nearly linear and aligned with the backazimuth (dotted line), which indicates null splitting. (g-h) Error contours for the rotation correlation (Figure 4g) and transverse component (Figure 4h) methods.

3. Results

Data processing and measurement procedures yielded 397 individual SKS arrivals ranked as either "good" or "fair" at MAGIC stations from ~107 events. The greater part of these measurements (65%) were null (nonsplit) arrivals. Null SKS arrivals exhibit linear uncorrected particle motion and indicate either a lack of anisotropy beneath the station, or that the initial polarization of an SKS phase passing through a single layer of anisotropy is equal to the apparent fast or "slow" direction. The slow direction is perpendicular to the apparent fast direction.
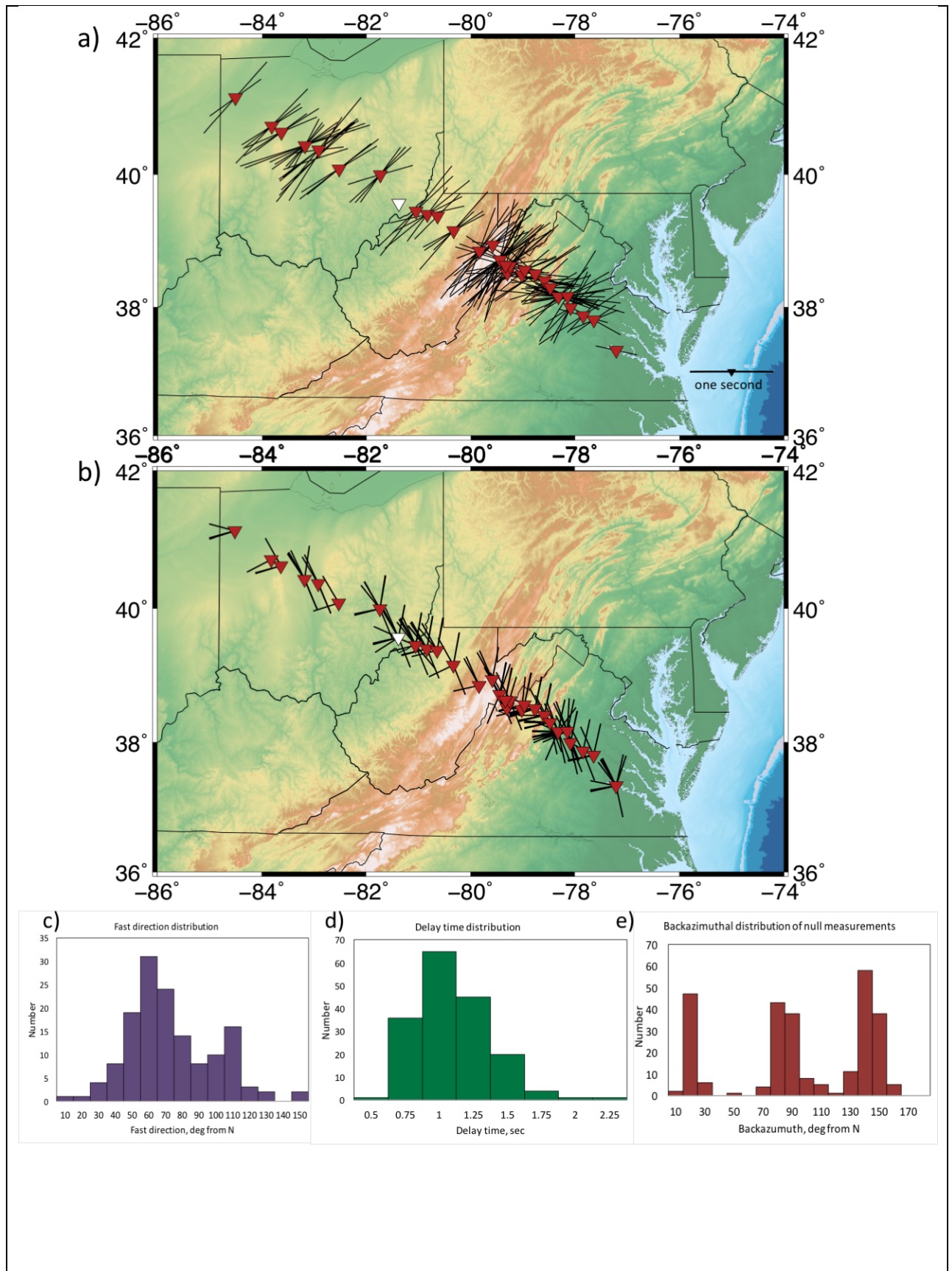
Figure 6. (a) Map of all nonnull SKS splitting paramater measured, plotted at individual MAGIC stations (red inverted triangles) using GMT (Wessel et al., 2015). Black bars indicate ϕ by orientation and δt by length. A scale point displays sample paramaters for ϕ = 90° and δt = 1.0 s. At one station, PVGR (white inverted triangle) in Lower Salem, Ohio, only null SKS arrivals were measured. (b) Map of null measurements recorded at individual MAGIC stations (stations plotting convention as in Figure 6a). Black tails indicate the backazimuth between the event and station along the great circle path. Tail lengths are uniform because there is no ϕ or δt associated with null splitting. (c) Histogram showing the distribution of all fast directions measured (modulo 180°), with peaks around 60° and 110°. (d) Histogram displaying the distribution of delay times measured using MAGIC data, with a peak around 1.0 s, a typical delay time for the Eastern U.S. (e) Histogram of the backazimuthal distribution of null measurements (modulo180°).

The average ϕ for the MAGIC array is 69° (modulo 180°, SD = 26°), with the histogram displaying a bimodal distribution with peaks around 60° and 110° (Figure 6c). A map of all SKS splitting parameters recorded (Figure 6a) reveals that stations in Ohio and West Virginia are dominated by SKS arrivals with a fast direction of ~60°, roughly parallel to the strike of the Appalachian range in West Virginia, whereas measurements taken from Virginia exhibit a more E-W orientation. A histogram of delay times (Figure 6d) shows a unimodal distribution around an average δt of 0.94 s (SD = 0.29 s), a typical result for continental regions (e.g., Silver, 1996; Fouch and Rondenay, 2006), yet less than observed SKS δt for the western U.S. where average delay times are as high as 2.0 s (e.g., Hongsresawat et al., 2015). A map of 258 null measurements is presented in Figure 6b. Tails are used to indicate the backazimuth between the event and station. Null measurements can help to highlight the apparent fast and slow directions associated with anisotropy, depending on the degree of backazimuthal coverage offered by the distribution of seismic activity. The MAGIC dataset exhibits fair backazimuthal coverage for a temporary deployment, although there are a few obvious gaps in coverage between 60° and 240° (see Figure 3b). A histogram of the backazimuthal distribution of null measurements (Figure 6e) shows peaks around 20°, 90°, and 145°. The peak around 20° corresponds to the slow

direction sometimes recorded at Virginia stations (ϕ = 110°). The peak around 90° corresponds to the ϕ sometimes recorded at stations in western Virginia. The peak around 140° - 150° corresponds to the average slow direction of stations in Ohio and West Virginia (ϕ = 60°).

To better describe the lateral variations in observed anisotropy, we have grouped MAGIC stations into three regions. Western stations (PAUL, ADAO, KENT, SUSI, AZZI, DENI, MUSK, PVGR, CDRF, NAZF, ALMA, PETO) are situated in the generally flat topography of the Central Lowland province and the Appalachian Plateaus, which cover eastern Ohio and the western half of West Virginia. Western stations exhibit a high number of null measurements (72%) and a consistent NE-SW trend in fast direction. A histogram of measured fast directions (Figure 7a) shows a unimodal distribution around 60°. Mountain stations (WIRE, RTSN, CABN, AND JSPR, CAKE, FOXP) are located in the high topography of the Valley and Ridge province of eastern West Virginia. Analysis of mountain station data resulted in a low number of null measurements relative to western and eastern stations (38%). A histogram of mountain station fast directions (Figure 7b) shows a bimodal distribution around 60° (similar to western stations) and a smaller peak around 100°. Eastern stations (TRTF, MOLE, LADY, INTX, WTMN, WINE, WLFT, BARB, YLDA, LBDL, BDEG) are located in Virginia. They cross the Great Valley subprovince of the Appalachian Valley and Ridge province, as well as the Blue Ridge, Piedmont, and Coastal Plain provinces (Roberts and Bailey, 2000). Eastern stations yielded mainly null splitting (70%), much like western stations. A histogram of fast directions (Figure 7c) shows a main peak around 110° and a smaller peak around 60°.
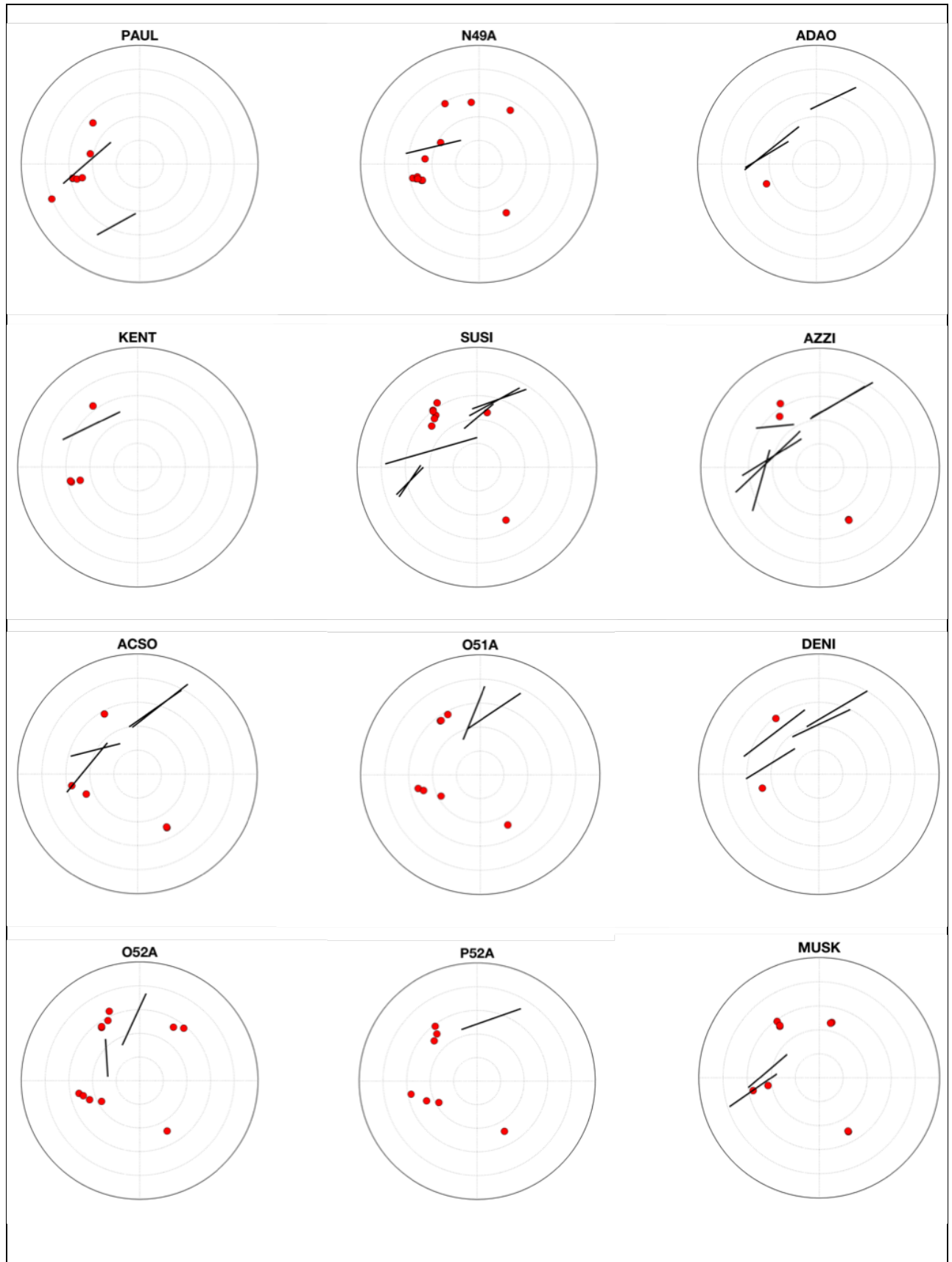
Stereoplots were made from MAGIC data, and combined with results from previous work (Long et al., 2016) to better illustrate single station splitting patterns along the MAGIC array (Figure 8). Twelve stations from the USArray were selected for inclusion because they fell within the path of the MAGIC array, in order to present the highest resolution of splitting patterns in a nearly straight path from BDEG (Paulding, Ohio) to T60A (Surry, Virginia). The stereoplots help in the interpretation of null measurements, revealing that eastern stations exhibit a number of null arrivals from a broader range of
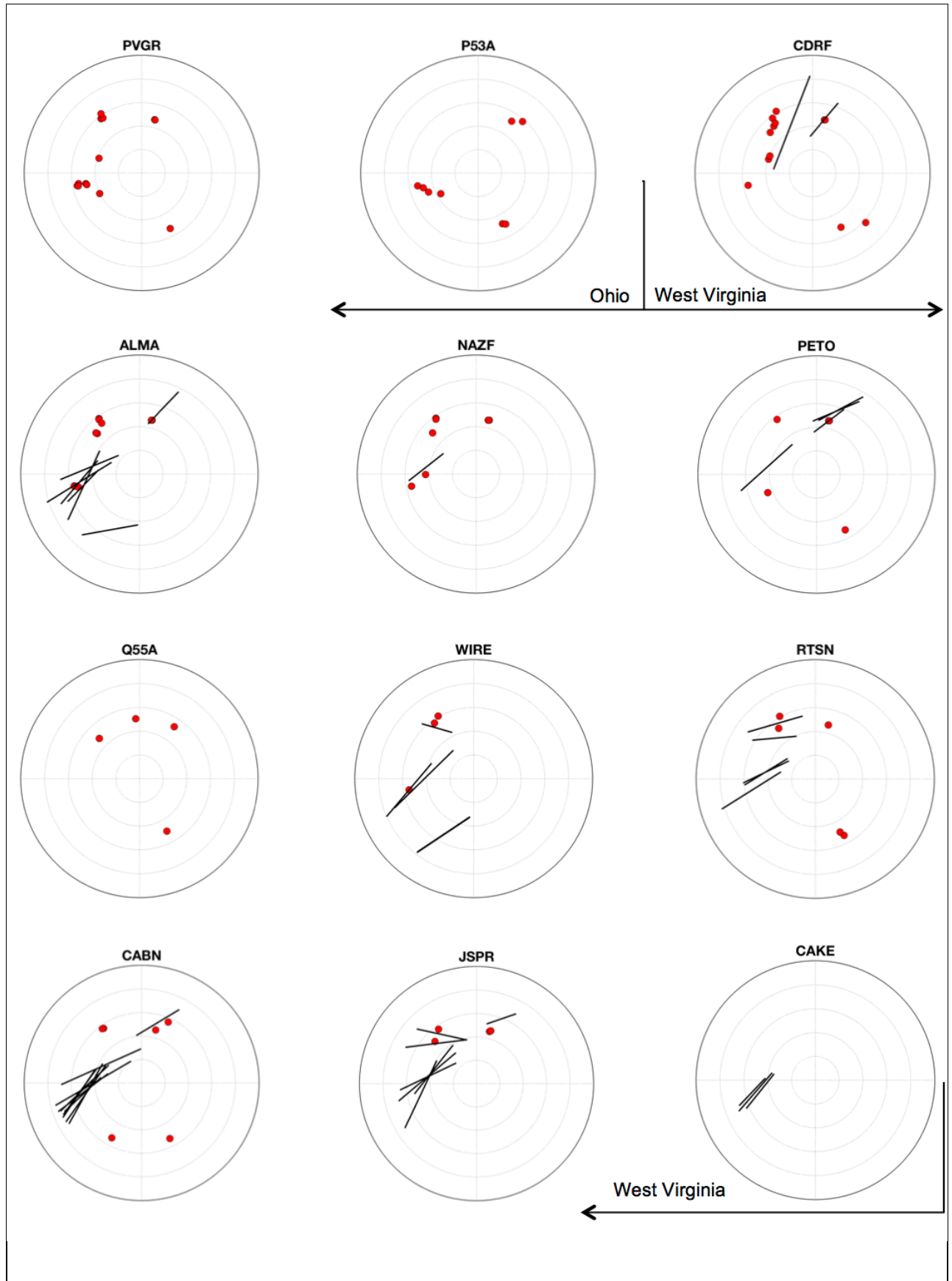
backazimuths. They also reveal at what point E-W fast directions begin to appear in mountain stations.
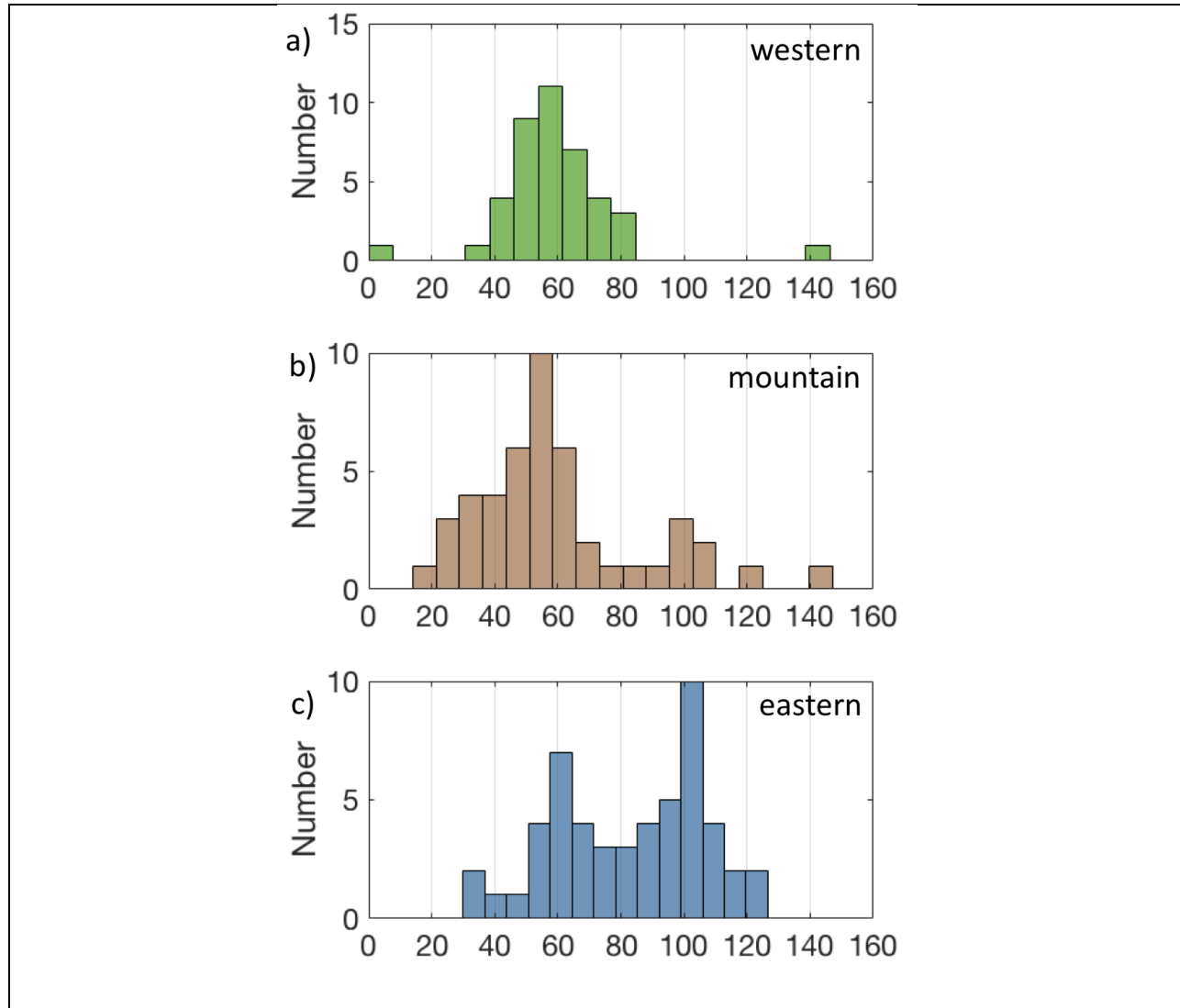
Figure 7. Histograms of measured fast directions, plotted by region (modulo 180°). (a) Western stations (PAUL, ADAO, KENT, SUSI, AZZI, DENI, MUSK, PVGR, CDRF, NAZF, ALMA, PETO) have a unimodal distribution of fast directions around 60°. (b) Mountain stations (WIRE, RTSN, CABN, AND JSPR, CAKE, FOXP) maintain the peak found in Ohio around 60° while displaying a few measurements where $\phi \sim 100°$. (c) Eastern stations in Virginia (TRTF, MOLE, LADY, INTX, WTMN, WINE, WLFT, BARB, YLDA, LBDL, BDEG) present a bimodal distribution of fast directions around 60° and 110°.

PAUL

N49A

ADAO

KENT

SUSI

AZZI

ACSO

O51A

DENI

O52A

P52A

MUSK

PVGR · P53A · CDRF

Ohio | West Virginia

ALMA · NAZF · PETO

Q55A · WIRE · RTSN

CABN · JSPR · CAKE

West Virginia

18

R56A   FOXP   MOLE

Virginia

TRTF   LADY   INTX

R57A   WTMN   WINE

WLFT   BARB   R58B
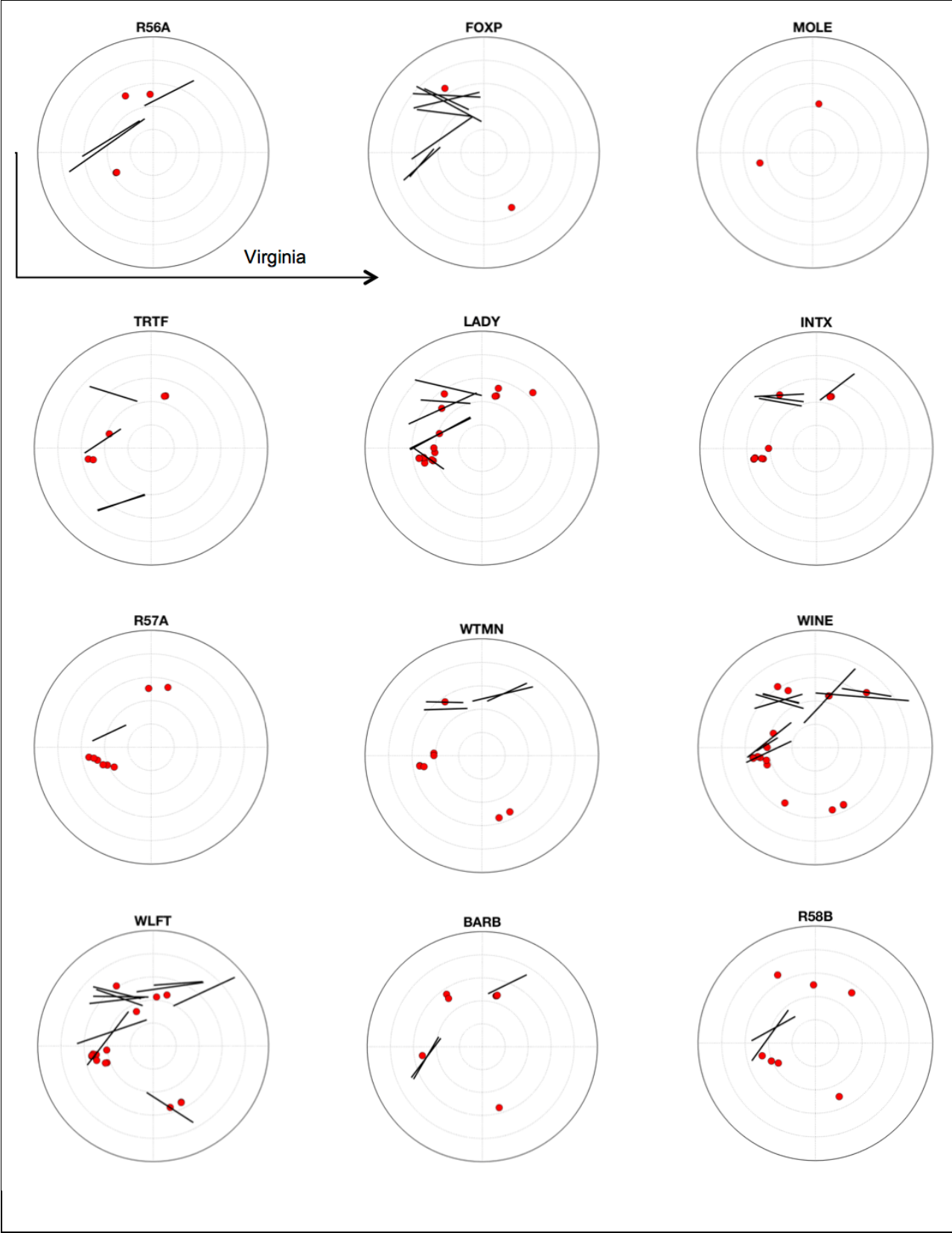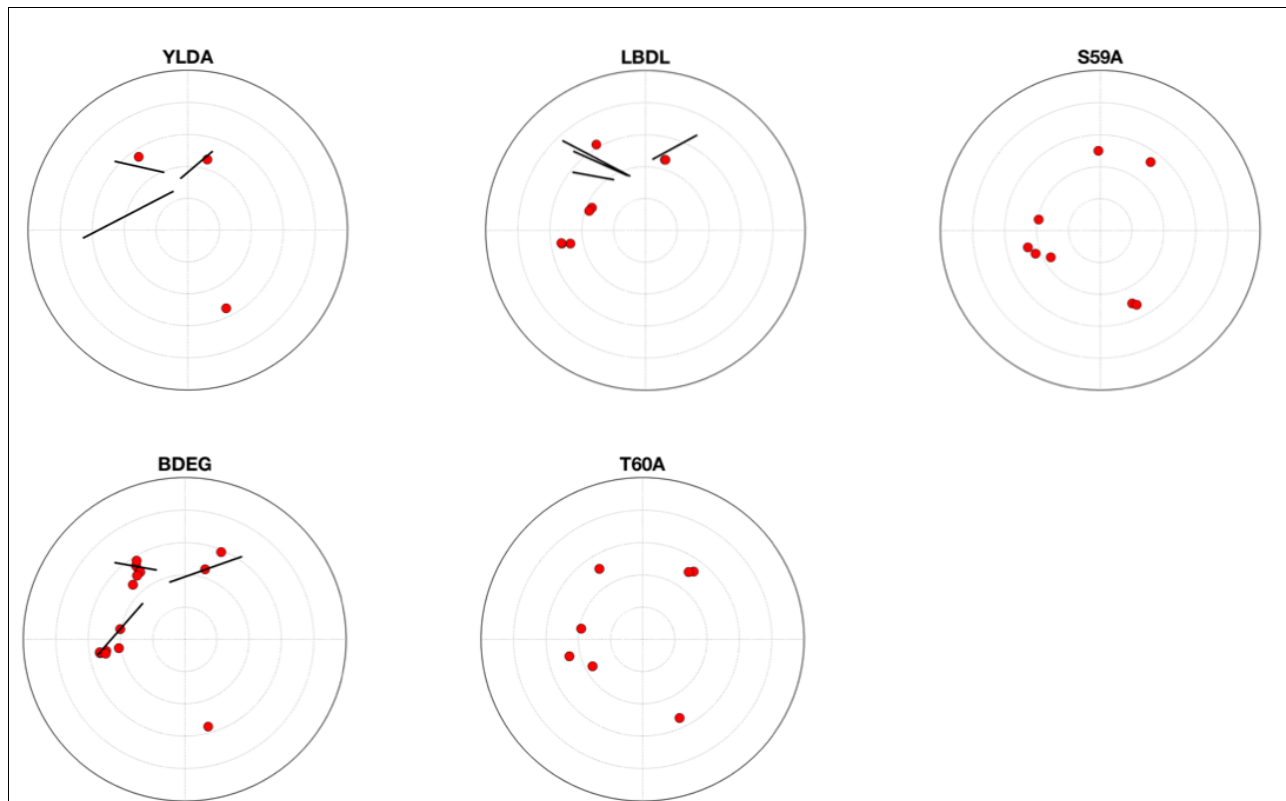
Figure 8. Single-station splitting patterns for all MAGIC stations, plus an additional 12 stations in the USArray (USArray Reference and USArray Transportable Array) (ACSO, N49A, O51A, O52A, P52A, P53A, Q55A, R56A, R57A, R58B, S59A, T60A) that fall within the general path of MAGIC stations using results from Long et al., 2016 and data from (Albuquerque Seismological Laboratory, 1990; Long and Wiita, 2013; USArray, 2003). Measurements are plotted as a function of backazimuth (angle from top of circle) and incidence angle (distance from center of circle). Non-null arrivals are plotted with black bars, indicating the fast direction (angle of bar) and delay time (length of bar). Null arrivals are plotted with red circles.
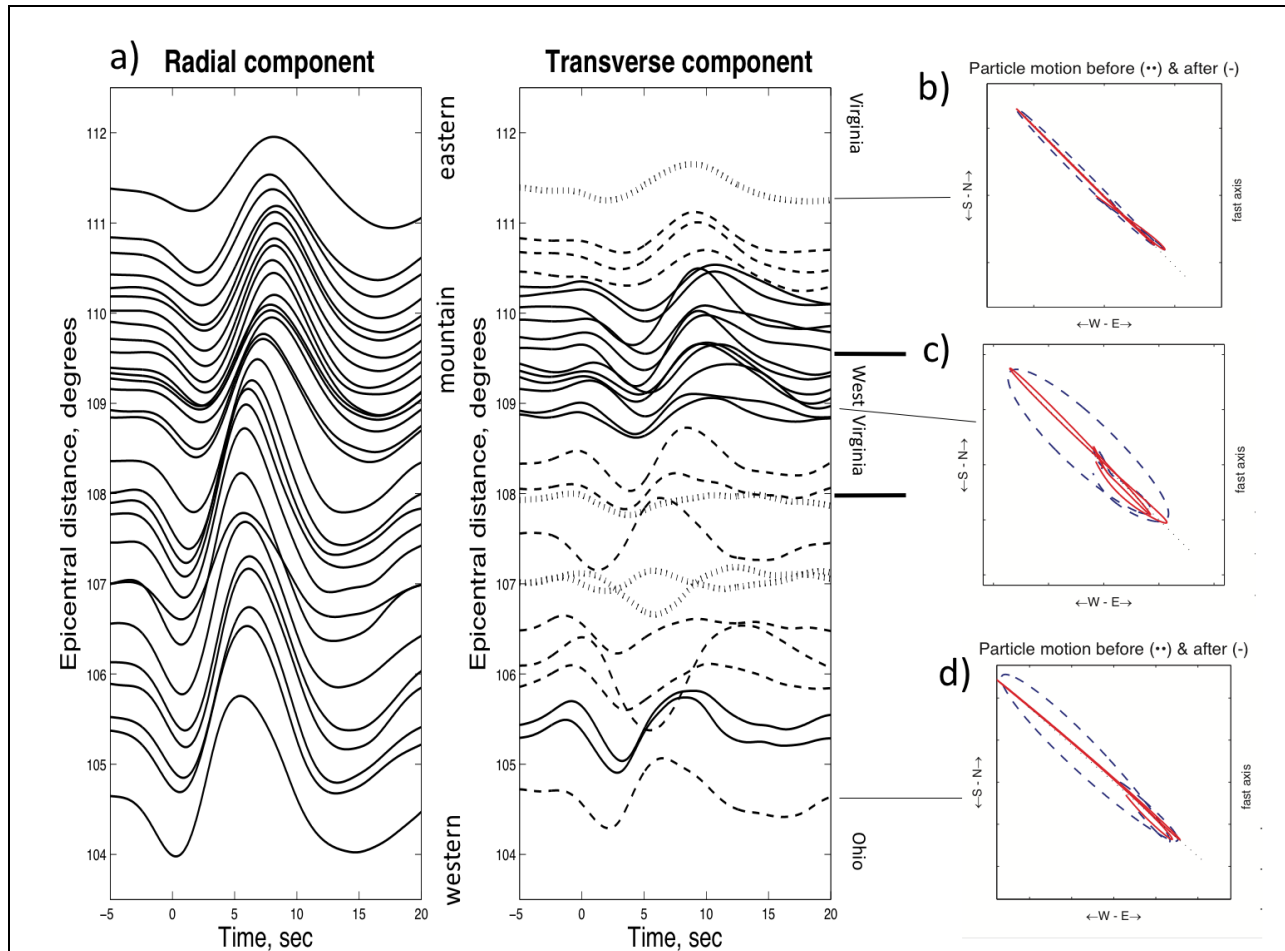
Figure 9. (a) Radial and transverse component record sections for MAGIC and USArray stations for an event originating from the Northern Mariana Islands on July 29, 2016 (Mw = 7.7, depth = 196 km, average backazimuth = 314°). Waveforms have been filtered to retain energy between 8 and 25 seconds, rotated to the backazimuth along the great circle path, aligned to the expected *SKS* arrival and plotted by epicentral distance from the event. Transverse components amplitudes have been multiplied by 2, and are plotted according to initial particle motion observed in SplitLab (Wüstefeld et al., 2008). Thick dotted lines (‖‖‖‖‖) represent an initial particle motion that is linear, as in Figure 9b. Solid lines represent an initial particle motion that is elliptical as in Figure 9c. Dashed lines represent initial particle motion that is not linear, yet less elliptical than Figure 9b. (b) *SKS* arrival at eastern station BDEG (Charles Lake, Virginia) with an initial particle motion that is linear (dashed blue line) and a corrected particle motion (the effects of splitting are removed

using the transverse component minimization method) that is linear (red line), indicating null splitting. The thin dotted line indicates the backazimuth. Figures 9c-9d follow plotting convention of 8b. (c) *SKS* arrival at mountain station CABN (Riverton, West Virginia), showing an initial particle motion that is elliptical and a corrected particle motion that is linear, indicating nonnull splitting. (d) *SKS* arrival at western station PAUL (Paulding, Ohio) with an initial particle motion that is weakly elliptical, and a corrected particle motion that is linear. This is typical of a "near-null" *SKS* arrival with weak splitting, where $\delta t < 0.5$ s, for which splitting parameters cannot be reliably constrained (eg., compare to Figure 4f, where $\delta t = 0.6s$).

Record sections of *SKS* arrivals have been included as a supplement to *SKS* splitting analysis. These record sections illustrate patterns in transverse component energy. For example, the record section from a 7.7 Mw event originating from the Northern Mariana Islands (Figure 9) illustrates very cohesive and elliptical, particle motion within the mountain region. This type of particle motion is typical of a nonnull splitting, but *SKS* analysis at 30 stations from this event resulted in only four high quality, well constrained *SKS* splitting measurements, because well resolved splitting parameters are rare. This fact makes record section analysis a valuable tool. Figures 10a – 10b show similar patterns as Figure 9, with mountain, and some western, stations exhibiting elliptical particle motions, and eastern stations showing mostly linear (null) particle motion. However, Figures 10c – 10d from events with backazimuths of 14° and 20° offer more complicated results, with all regions recording waveforms with similar energy and elliptical particle motion.
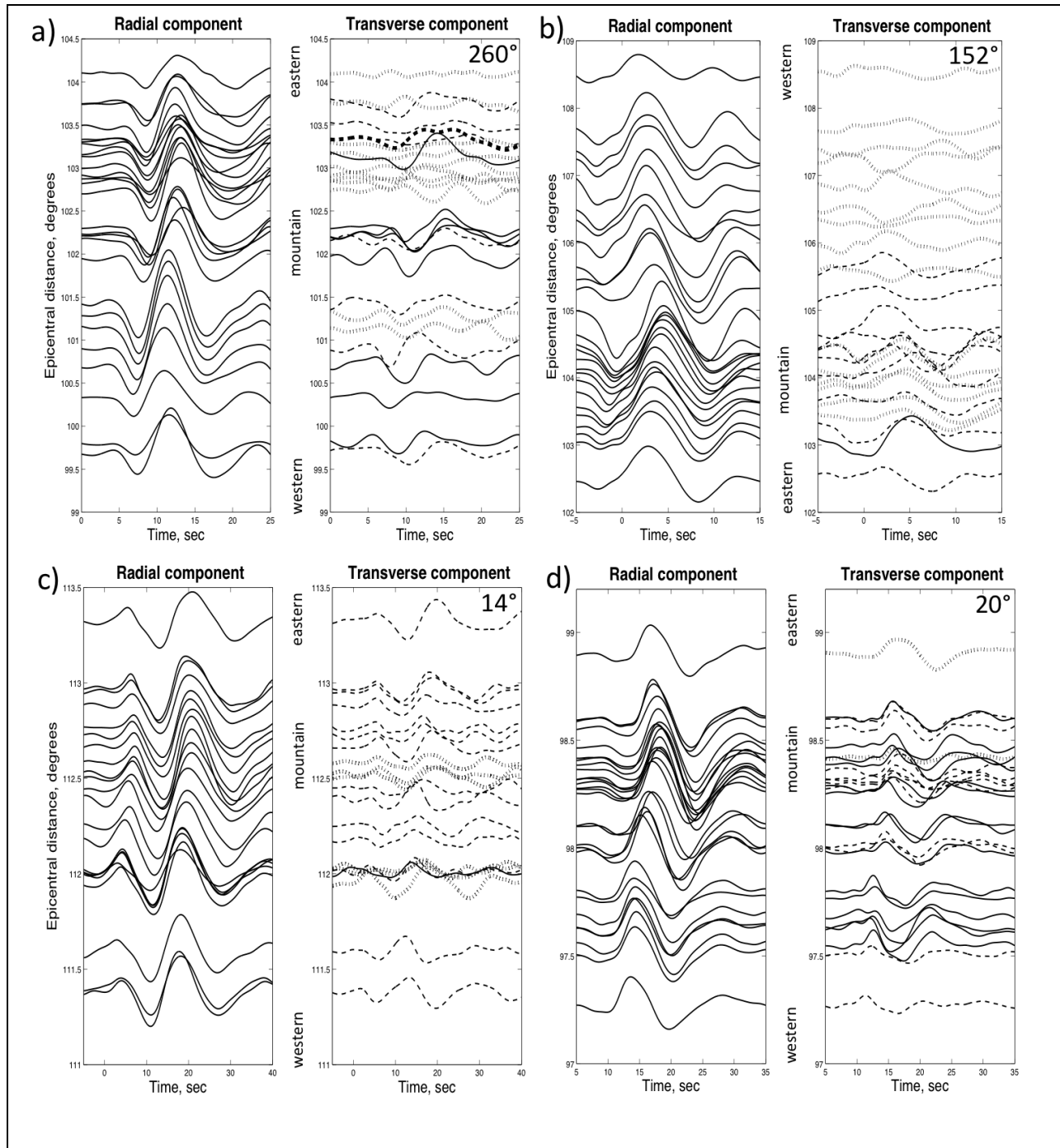
Figure 10. Four record sections showing the radial and transverse component for MAGIC and select USArray stations from a range of backazimuths (printed in top right corner of transverse component). Waveforms have been processed and plotted according to the conventions of Figure 9. (a) Record section for an event originating near Hihifo, Tonga on April 7, 2015 (Mw = 6.3, depth = 30 km, average backazimuth = 260°). (b) Record section

for an event originating near the South Sandwich Islands on May 28, 2016 (Mw = 7.2, depth = 78 km, average backazimuth = 152°). (c) Record section for an event originating near Kodari, Nepal on May 12, 2015 (Mw = 7.3, depth = 15 km, average backazimuth = 14°). (d) Record section for an event originating near Sary Tash, Kyrgyzstan on June 26,2016 (Mw = 6.4, depth = 13 km, average backazimuth = 20°).

4. Discussion

Recent studies of *SKS* splitting using TA data have revealed the complex nature of anisotropy beneath eastern North America. They provide evidence for multiple layers of anisotropy and likely contributions from lithospheric and asthenospheric deformation (eg., Hongsresawat et al., 2015; Liu et al., 2014; Long et al., 2016; Refayee et al., 2014; Yang et al., 2014). Unfortunately, the source of upper mantle anisotropy cannot be determined using *SKS* splitting alone. *SKS* splitting parameters are path integrated measurements from a near vertical phase with poor depth resolution (Long and Silver, 2009). Additionally, our analysis cannot resolve splitting with delay times less than 0.5 s. Despite these drawbacks, aggregated splitting measurements from a dense array can provide excellent resolution of lateral changes in upper mantle anisotropy (Long and Silver, 2009).

The arrival of the USArray Transportable Array to eastern North America has provided a large store of data from ~400 stations. Long et al. (2016) identify regional trends in Mid-Atlantic anisotropy from *SKS* splitting, which we have combined with MAGIC *SKS* splitting data. A map of single station averages (Figure 11a) displays good agreement between most of our measurements and previous work. TA stations near western and mountain stations exhibit average fast directions roughly parallel to the strike of the Appalachians and delay times of ~1.0 s. Curiously, Western stations PVGR (MAGIC data) and P53A (TA data) near the Ohio, West Virginia border offered only nonsplit measurements from a relatively wide range of backazimuths (see Figure 8 for stereoplots from these stations). This is interesting given the coherent splitting observed at surrounding stations. This could indicate a small region of isotropic upper mantle and crust, or it could be that more time was needed to collect a high quality split *SKS* arrival than the two deployments allowed for.
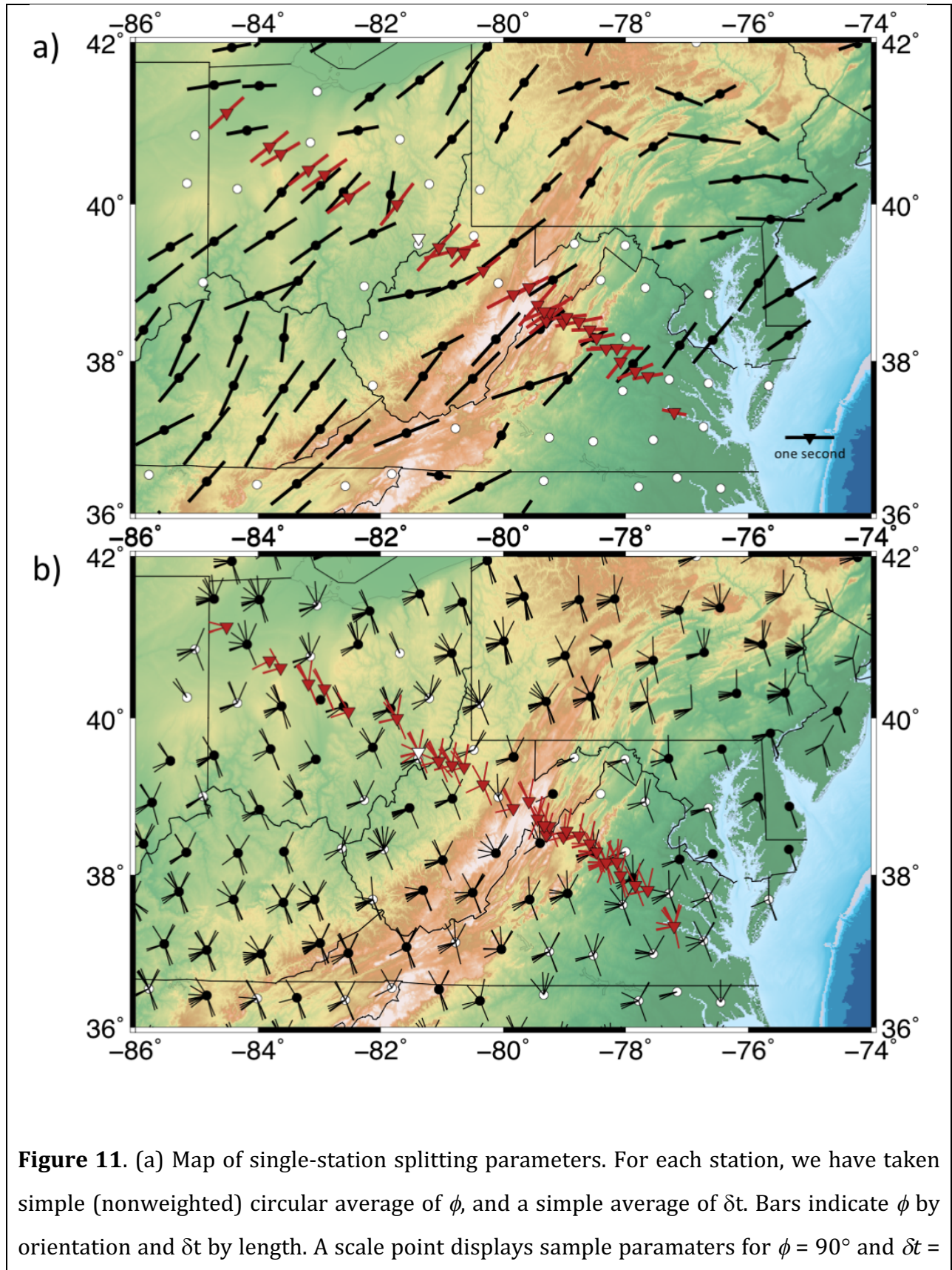
Figure 11. (a) Map of single-station splitting parameters. For each station, we have taken simple (nonweighted) circular average of ϕ, and a simple average of δt. Bars indicate ϕ by orientation and δt by length. A scale point displays sample paramaters for $\phi = 90°$ and $\delta t =$

1.0 s. MAGIC stations (red inverted triangles) and results (red bars) are superimposed on a map of single-station averages from previous work using data from the USArray Transportable Array (TA) (Long et al., 2016) using GMT (Wessel et al., 2015). At one MAGIC station, PVGR (white inverted triangle) in Lower Salem, Ohio, only null *SKS* arrivals were measured. TA stations (black circles) and single-station averages (black bars) demonstrate the general pattern of anisotropy beneath the Eastern U.S. White circles mark TA stations where at least five null *SKS* arrivals were recorded, and no "good" or "fair" split arrivals were measured (Long et al., 2016). (b) Map of indivudual null measurements recorded at MAGIC and TA stations (stations plotting convention as in Figure 7a).

It is also possible that small-scale heterogeneities in anisotropic structure result in anisotropy too weak to measure at PVGR and P53A (Long et al., 2010). There is some evidence for this in record section. A close look at the transverse component record from an event near the Northern Mariana Islands (Figure 9) illustrates a sharp transition from clear and coherent elliptical initial particle motion (indicative of strong splitting where δt = 1.0 s) at mountain stations to less elliptical particle motion, indicative of weak splitting (δt < 0.5 s, see Figure 4f for an example of initial particle motion when δt = 0.6s) in western stations. Station P53A was not running at this time, but station PVGR is plotted just above the 108° epicentral distance tick with and initial particle motion indicative of weak splitting.

Mountain stations exhibit the highest agreement with TA results from Long et al. (2016). MAGIC and TA results give an average ϕ of 60° (*SD* = 27) and 61°, respectively, illustrating the close relationship between the high topography of the Appalachian mountain chain and observed anisotropy, including the rotation of ϕ values to an E-W trend near the Pennsylvania Salient (Figure 11a). This observation is the strongest evidence suggesting that a region of frozen-in lithospheric deformation associated with Appalachian orogenesis exists beneath the high topography of the Valley and Ridge province. At the same time, there is evidence suggesting probable contribution from crustal deformation (depth = 8-10 km) with a similar ϕ to our study (Lin and Schmandt, 2014), suggesting that the lithosphere and crust may have deformed coherently. Additionally, a comparison

26

between the average fast direction of mountain stations ($\phi = 60°$) and APM points to a likely contribution from present-day mantle flow (Long et al., 2016), adding to the problem's complexity.

Data from eastern stations shed new light on the Atlantic Coastal Plain. A map of single stations averages (Figure 11a) shows a coherent rotation of the average ϕ to about 80°. These findings confirm results from the four Virginia TA stations within the path of the MAGIC array (Figure 11a), while at the same time questioning previous findings suggesting that northern Virginia is dominated by null splitting. This discrepancy could be attributed to the underlying structure, or the fact that many MAGIC stations in this region recorded 36 months of data versus the 18-24 months of data available from TA stations in northern Virginia when the previous analysis was completed (Long et al., 2016). Single station averages from eastern stations are also misleading. A histogram from this region (Figure 7c) clearly shows a bimodal distribution of ϕ with peaks around 60° and 110°, indicating there are likely multiple layers of anisotropy, a common phenomenon in North America as indicated by surface wave models (eg., Deschamps et al., 2008) and receiver function analysis (eg., Wirth and Long, 2014). We find that measured fast directions are complemented by the distribution of null splitting results. Figure 11b shows a combination of null results from this study and Long et al. (2016) at individual stations. Null results from eastern stations are similar to the distribution of experiment-wide results (Figure 6c), with peaks centered around 15°, 80° and 150° (modulo 180°). The peaks around 80° and 15° correspond the common fast (where $\phi \sim 80$ from a minority of measurements) and slow (where $\phi \sim 110°$ from a majority of measurements) directions reported from eastern stations. However, the peak around 150° corresponds to a slow direction (when $\phi = 60°$), which is present across *all* regions.

Stereoplots arranged from western to eastern stations illustrate the shared anisotropy of these regions, which is obscured by maps of single-station averages and individual measurements. A close look at Figure 8 shows that E-W trending ϕ measurements, which dominate eastern stations, can be found as far west as mountain stations WIRE, RTSN, and JSPR. Similarly, a NE-SW trending ϕ was recorded at *all* stations, although this splitting pattern becomes rare for the eastern half of Virginia (see Figure 8).

Complex anisotropy will often result in variations in apparent splitting parameters with backazimuth (Long and Silver, 2009). There is some evidence for this in stereoplots (Figure 8), although more study is needed. Mountain stations exhibiting an E-W trending fast direction (eg., WIRE, RTSN, JSPR) for events with a backazimuth of ~330°. E-W splitting patterns at eastern stations are similar, and often come from a backazimuth of ~330° or ~45° (eg., LADY, WINE, WLFT).

The fact that nearly all stations in the MAGIC array share some degree of NE-SW oriented anisotropy (ϕ = 60°) helps to explain the surprising agreement between MAGIC stations observed in the record sections found in Figures 10c-10d. An anisotropic layer with a ϕ of 60° would be most strongly detected using data from events with a backazimuth offset by 45° from 60° (eg., 15°, 105°, 195°, and 285°). Figures 10c and 10d have an average backazimuth of 14° and 20°, respectively, and record sections of MAGIC transverse component energies and initial particle motions (as measured in SplitLab) reveal coherent results for all stations. Figure 10c illustrates particle motions typical of weak splitting at nearly all stations for a 7.3 Mw event originating near Kodari, Nepal on May 12, 2015. Figure 10d shows initial particle motions suggesting a mixture of strong and weak splitting at all stations from a 6.4 Mw event originating near Sary Tash, Kyrgyzstan on June 26, 2016. These results suggest some level of shared upper mantle anisotropy between western, mountain, and eastern stations.

Eastern North America holds a great deal of complexity and variability in anisotropic structure, as shown from recent *SKS* splitting measurements taken from TA data. Long et al. (2016) offer the first comprehensive analysis of *SKS* splitting patterns across this region, and their results define broad regions of coherent splitting patterns. Our data set for stations in the MAGIC experiment help identify how these regions are delineated in terms of anisotropic structure. SKS splitting patterns documented in this study support the conclusion that anisotropy in the Mid-Atlantic Appalachians is a complicated mix of frozen-in lithospheric deformation and present-day flow in the asthenosphere. More work is needed to fully evaluate the degree of influence each of these sources has on observed anisotropy. Moving forward, the high resolution offered by the dense MAGIC instrument array will provide valuable data for use in anisotropic receiver

function analysis, measurements of surface wave dispersion, and other techniques that can constrain models of upper mantle flow beneath North America.

5. Summary

We evaluated record sections of *SKS* arrivals and measured splitting of *SKS* phases using seismic data collected by the Mid-Atlantic Geophysical Integrative Collaboration. Our *SKS* splitting measurements agree with previous work. Significant findings include a general E-W trend in splitting patterns to the west and within the Appalachian Mountains that match the strike of the high topography. Delay times of ~1.0 s (*SD* = 0.3 s) did not vary much within our region of study, but there were sharp lateral changes in anisotropy. Virginia stations crossing the Blue Ridge, Piedmont, and Atlantic Costal provinces exhibit more complicated splitting, with patterns presenting both a NE-SW and E-W fast direction and suggesting the possibility of multilayered anisotropy. Record sections of *SKS* arrivals at MAGIC stations reveal very coherent splitting for stations within the Appalachian Mountains. Stereo plots of splitting patterns work to highlight lateral transitions in anisotropic structure and the ways in which previously defined regions of coherent anisotropy overlap. Delay times from this work support previous findings pointing to there being both lithospheric and asthenospheric contributions to observed anisotropy in eastern North America.

6. Acknowledgments

References

Albuquerque Seismological Laboratory, A. U., 1990, United States National Seismic Network, International Federation of Digital Seismograph Networks, p. Other/Seismic Network. doi: 10.7914/SN/US

Aragon, J. C., Long, M. D., Benoit, M. H., Kirby, E., and King, S. D., SKS splitting beneath the MAGIC FlexArray experiment, *in* Proceedings AGU Fall Meeting, San Francisco, CA, 2015, AGU, p. DI21A-2594.

Aragon, J. C., Long, M. D., Benoit, M. H., and Servali, A., Seismic anisotropy in the upper mantle beneath the MAGIC array, mid-Atlantic Appalachians: Constraints from SKS splitting and quasi-Love wave propagation, *in* Proceedings AGU Fall Meeting, San Francisco, CA, 2016, p. T51G-3004.

Cawood, P. A., and Buchan, C., 2007, Linking accretionary orogenesis with supercontinent assembly: Earth-Science Reviews, v. 82, no. 3-4, p. 217-256. doi: 10.1016/j.earscirev.2007.03.003

Deschamps, F., Lebedev, S., Meier, T., and Trampert, J., 2008, Stratified seismic anisotropy reveals past and present deformation beneath the East-central United States: Earth and Planetary Science Letters, v. 274, no. 3-4, p. 489-498. doi: 10.1016/j.epsl.2008.07.058

Fenneman, N. M., and Johnson, D., 1946, Physical divisions of the United States: US Geol: Survey map, v. 1.

Fouch, M. J., 2006, Imaging continental deformation: EarthScope in the filed and the classroom: IRIS Newsletter, no. 3.

Hatcher, R. D., Jr., 2010, The Appalachian orogen: A brief summary, *in* Tollo, R. P., Bartholomew, M. J., Hibbard, J. P., and Karabinos, P. M., eds., From Rodinia to Pangea: the Lithotectonic Record of the Appalachian Region, Volume 206, p. 1-19. doi: 10.1130/2010.1206(01)

Hoffman, P. F., Randall, J. S., and Zelinsky, W., 2016, North America, Encyclopædia Britannica, Encyclopædia Britannica, inc.

Hongsresawat, S., Panning, M. P., Russo, R. M., Foster, D. A., Monteiller, V., and Chevrot, S., 2015, USArray shear wave splitting shows seismic anisotropy from both lithosphere and asthenosphere: Geology, v. 43, no. 8, p. 667-670. doi: 10.1130/g36610.1

Karato, S.-i., Jung, H., Katayama, I., and Skemer, P., 2008, Geodynamic significance of seismic anisotropy of the upper mantle: New insights from laboratory studies, Annual Review of Earth and Planetary Sciences, Volume 36, p. 59-95. doi: 10.1146/annurev.earth.36.031207.124120

Lin, F.-C., and Schmandt, B., 2014, Upper crustal azimuthal anisotropy across the contiguous US determined by Rayleigh wave ellipticity: Geophysical Research Letters, v. 41, no. 23, p. 8301-8307. doi: 10.1002/2014gl062362

Liu, K. H., Elsheikh, A., Lemnifi, A., Purevsuren, U., Ray, M., Refayee, H., Yang, B. B., Yu, Y., and Gao, S. S., 2014, A uniform database of teleseismic shear wave splitting measurements for the western and central United States: Geochemistry Geophysics Geosystems, v. 15, no. 5, p. 2075-2085. doi: 10.1002/2014gc005267

Long, M. D., 2010, Frequency-dependent shear wave splitting and heterogeneous anisotropic structure beneath the Gulf of California region: Physics of the Earth and Planetary Interiors, v. 182, no. 1-2, p. 59-72. doi: 10.1016/j.pepi.2010.06.005

Long, M. D., Benoit, M. H., Chapman, M. C., and King, S. D., 2010, Upper mantle anisotropy and transition zone thickness beneath southeastern North America and implications for mantle dynamics: Geochemistry Geophysics Geosystems, v. 11. doi: 10.1029/2010gc003247

Long, M. D., Jackson, K. G., and McNamara, J. F., 2016, SKS splitting beneath Transportable Array stations in eastern North America and the signature of past lithospheric deformation: Geochemistry Geophysics Geosystems, v. 17, no. 1, p. 2-15. doi: 10.1002/2015gc006088

Long, M. D., and Silver, P. G., 2009, Shear Wave Splitting and Mantle Anisotropy: Measurements, Interpretations, and New Directions: Surveys in Geophysics, v. 30, no. 4-5, p. 407-461. doi: 10.1007/s10712-009-9075-1

Long, M. D., and Wiita, P., 2013, Mid-Atlantic Geophysical Integrative Collaboration, International Federation of Digital Seismograph Networks, p. Other/Seismic Network. doi: doi:10.7914/SN/7A_2013

MATLAB, 2012, MATLAB Release 2012b: Massachusetts, United States, The MathWorks, Inc. .

Refayee, H. A., Yang, B. B., Liu, K. H., and Gao, S. S., 2014, Mantle flow and lithosphere-asthenosphere coupling beneath the southwestern edge of the North American craton: Constraints from shear-wave splitting measurements: Earth and Planetary Science Letters, v. 402, p. 209-220. doi: 10.1016/j.epsl.2013.01.031

Roberts, C., and Bailey, C. M., 2000, Physiographic Map of Virginia Counties: College of William and Mary.

SAC, 1995, Siesmic Analysis Code version 101.6A, Regents of the University of California.

Thorne, M., 2015, SACLAB, The University of Utah.

USArray, T. A., 2003, USArray TransporableArray, International Federation of Digital Seismograph Networks, p. Other/Seismic Network. doi: 10.7914/SN/TA

Wagner, L. S., Long, M. D., Johnston, M. D., and Benoit, M. H., 2012, Lithospheric and asthenospheric contributions to shear-wave splitting observations in the southeastern United States: Earth and Planetary Science Letters, v. 341, p. 128-138. doi: 10.1016/j.epsl.2012.06.020

Wessel, P., Smith, W. H. F., Scharroo, S. R., Luis, J., and Wobbe, F., 2015, GMT Generic Mapping Tools, Volume 5.2.1. doi: gmt.soest.hawaii.edu

Wirth, E. A., and Long, M. D., 2014, A contrast in anisotropy across mid-lithospheric discontinuities beneath the central United States-A relic of craton formation: Geology, v. 42, no. 10, p. 851-854. doi: 10.1130/g35804.1

Wüstefeld, A., Bokelmann, G., Zaroli, C., and Barruol, G., 2008, SplitLab: A shear-wave splitting environment in Matlab: Computers & Geosciences, v. 34, no. 5, p. 515-528. doi: 10.1016/j.cageo.2007.08.002

Yang, B. B., Gao, S. S., Liu, K. H., Elsheikh, A. A., Lemnifi, A. A., Refayee, H. A., and Yu, Y., 2014, Seismic anisotropy and mantle flow beneath the northern Great Plains of North America: Journal of Geophysical Research-Solid Earth, v. 119, no. 3, p. 1971-1985. doi: 10.1002/2013jb010561